Infrared spectroscopy of astrophysically relevant hydrocarbons

Doney, K.D.

1

INTRODUCTION

Hydrocarbons play an important role in the chemistry of a variety of astronomical environments from the diffuse interstellar medium to dense hydrocarbon atmospheres of solar system bodies (*e.g.*, Titan or Jupiter) and exoplanets. For most astronomical objects, the determination of chemical abundances, and consequently an understanding of the chemical evolution relies upon the observation of molecular spectra. However, to date astronomical models need to make assumptions, because not all of the molecules expected to participate in the reaction pathways have been observed. This is due, in part, to a lack of accurate line position data, which is needed for unambiguous identification. This thesis focuses on the study of the infrared spectroscopy of hydrocarbons, from *ab initio* calculations to high-resolution laboratory measurements to astronomical observations, in order to fill in some of these gaps.

1.1 INTRODUCTION

Hydrocarbons (with the general formula C_nH_m) are a particularly important class of molecules. Carbon's ability to form sp, sp^2, and sp^3 hybridized orbitals, and to undergo catenation (σ bonding between carbon atoms) allows hydrocarbons to form complex and geometrically diverse molecules. In pure carbon molecules, this leads to the physical differences observed between graphene and diamonds. On Earth hydrocarbons are primarily found in their saturated form, as natural gas or petroleum. As such, their predominant use is as a combustible fuel source - directly for heating, or to create electrical energy in power plants. Hydrocarbons in either their saturated or unsaturated forms are also the base molecules in organic synthesis, and are the structural basis of most biological molecules, *e.g.*, fatty acids [C_mH_nCOOH] and sugar [$C_6H_{12}O_6$] molecules.

In most astronomical environments, such as the interstellar medium (ISM) or circumstellar shells, the conditions are much harsher than on Earth, and as a result the chemistry and the stability of molecules is vastly different than that seen on Earth. For example, in the diffuse interstellar medium the low temperature (~10 - 100 K) and the low density (~10 - 100 particles/cm^3) allow unstable molecules, such as CH^+, to live for hundreds of years; while in the laboratory it may only last for fractions of a second. As such, the typical chemical formation mechanisms used to synthesize hydrocarbon molecules in "bench-top chemistry" do not work in astronomical environments. Instead, simplified reaction schemes are invoked to explain the observed presence of such molecules. The mechanisms are limited to: radiative association, dissociative recombination, ion-neutral and radical-neutral reactions, photodissociation, photoionization, and grain mediated reactions (Wakelam et al., 2012). Even with the simplified chemistry, around 200 molecules have been detected in astronomical objects, and a vast majority of them are unsaturated hydrocarbons or their O-, N-, S-bearing derivatives (Müller et al., 2005).

1.1.1 *Astronomical formation of hydrocarbons*

Based on the wide range of environments where hydrocarbons have been observed: planetary atmospheres (Kim et al., 1985; Waite et al., 2007), ejecta of evolved stars (Winnewisser & Walmsley, 1978; Cernicharo & Guélin, 1996), protoplanetary nebulae (Cernicharo et al., 2001; Malek et al., 2012), molecular clouds (Bell et al., 1999; Araki et al., 2017), HII regions (Allamandola et al., 1989), and protoplanetary disks (Gibb et al., 2007), one prevailing condition for high abundances of hydrocarbon formation is high density. Current astronomical models and theories assume simple hydrocarbons, *e.g.*, acetylene [H_2C_2] and methane [CH_4] (through sequential H-addition reactions), along with polycyclic aromatic hydrocarbons (PAHs) are formed in the atmospheres of dying red giant (or asymptotic giant branch, A.G.B.) stars under combustion-like conditions. In such cases, the HACA (hydrogen abstraction, carbon addition) model is the principle formation mechanism (Cherchneff, 2011; Agúndez, M. et al., 2017). These molecules are then ejected into the ISM were they become part of molecular clouds.

Gas-phase reactions are unlikely to form complex molecules unless in high density environments. In most cases molecules subsequently freeze out onto dust grains, such as in protoplanetary disks, where they undergo various photoprocessing and radical-radical reactions to form complex organic molecules (COMs). Such reaction schemes are thought to be the source of molecules like ethanol [C_2H_5OH] or glycolaldehyde [$HC(O)CH_2OH$] (Chuang et al., 2016). In dense environments with a nearby radiation source, such as warm core molecular clouds or the atmospheres of planets, long hydrocarbons chains like diacetylene [HC_4H] or benzene [C_6H_6] can be formed through gas-phase ion-neutral reactions (Figure 1.1; Smith (1992); McEwan et al. (1999); Sakai & Yamamoto (2013)).

Comparison of observed molecular abundances with those predicted from models gives insight into the reaction pathways, and thus the chemistry taking place in the different astronomical environments. Since molecular formation mechanisms are typically branched, with the branching

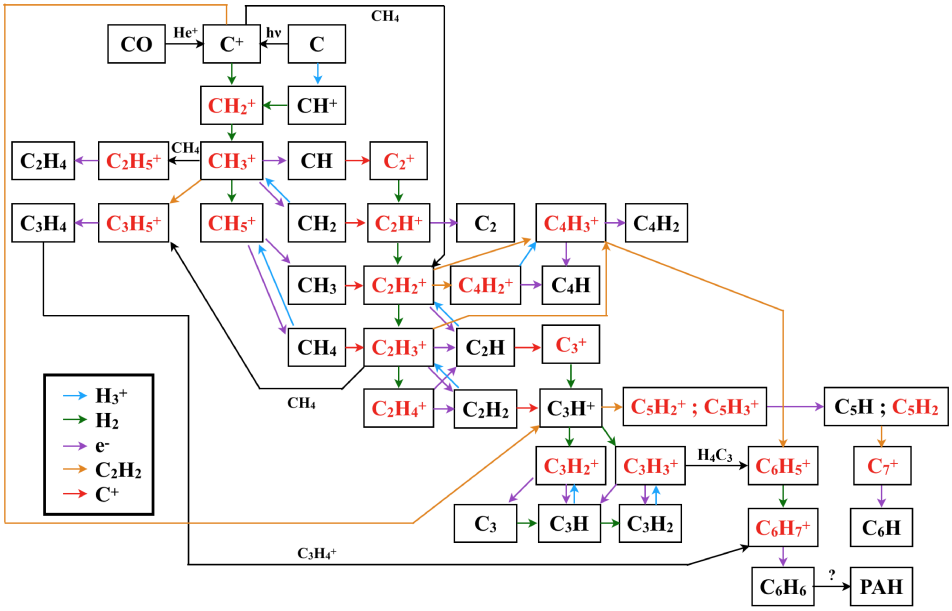

Figure 1.1: Part of the ISM gas-phase hydrocarbon reaction network based on Smith (1992); McEwan et al. (1999); Sakai & Yamamoto (2013). Molecules labeled in black have been detected spectroscopically in space, while molecules labeled in red have yet to be detected.

ratios temperature and pressure dependent, knowing the abundance of different molecules in the network can infer the how, when, and where these molecules were produced. Studying the abundance and spatial distribution of chemicals can also give direct diagnostics of the physical conditions of the astronomical environment. For example, the relative intensities of *K*'-subbands in a symmetric top molecule such as propyne [C_3H_4] or methyl cyanide [CH_3CN] probes the kinetic temperature (Churchwell & Hollis, 1983), or the gas density can be probed based on the presence of particular molecules in the gas-phase, like hydrogen cyanide [HCN] or the formyl cation [HCO^+] (Papadopoulos, 2007; van Kempen et al., 2009).

In nearby objects, *i.e.*, solar system objects where probes can be sent, the chemistry can be inferred from the chemical abundances determined by mass spectrometry of atmospheric or soil samples. In such cases, cationic hydrocarbons have been detected in relatively high abundances compared to their neutral species (Waite et al., 2007), suggesting the cationic-neutral formation mechanism is reasonable under high density and temperature conditions of planetary atmospheres. However, most astronomical objects are light years away, and understanding of their chemistry requires remote detections through emission or absorption spectroscopy. Unambiguous identification of a particular molecule can be accomplished through observation of its unique rotational transitions (typically in the microwave spectral range), or through observation of the ro-vibrational transitions (typically in the infrared (IR) spectral range). To date, few ionic species have been observed spectroscopically in the interstellar or circumstellar medium (Müller et al., 2005), and as such, the gas-phase ion-neutral formation mechanism is difficult to prove in distant environments.

Recent advancements in resolution of astronomical spectra, with instruments such as the Atacama Large Millimeter Array (ALMA) in the submillimeter/THz observations and CRIRES+ in the IR, mean that new forests of "weak" molecular transitions can now be observed. Unfortunately, some of the observed transitions cannot be assigned to any known molecular transition (Cernicharo et al., 2013). The non-detections can be attributed, in part, to a lack of accurate line positions for

the proposed molecules.

Accurate line positions for different molecular transitions can be obtained from high level *ab initio* calculations or from experimental measurements. While current *ab initio* theory can predict ground electronic state vibrational frequencies and rotational constants (A, B, and C) to within a few percent, experimental measurements are still required to determine the true value. In the past few decades, experimental techniques including cavity enhanced and cavity ring-down spectroscopy have improved the detection sensitivity such that transitions can be measured even for species with low molecular concentrations (O'Keefe & Deacon, 1988). There have also been advances in transient specie production with plasma discharge sources making *in situ* observation of unstable hydrocarbons possible (Motylewski & Linnartz, 1999).

In many cases, the infrared transitions of molecules are intrinsically stronger than their pure rotational transitions, and in some cases, *e.g.*, centrosymmetric molecules, pure rotational transitions are forbidden. As such, in order to measure new transitions of astrophysically relevant hydrocarbons, which are typically produced in low concentrations under laboratory conditions, we will focus on their strong C-H ro-vibrational transitions, a region that is accessible with precise laser systems in the laboratory and astronomical telescopes.

1.2 THEORY OF RO-VIBRATIONAL SPECTROSCOPY

Molecular spectroscopy is used to understand the nature of nuclear and electronic motions of a molecule by observing the interactions of the molecule with radiation. The absorption or emission of a photon with energy $h\nu$ by a molecule results in changes in its energy state, which can be observed as spectral lines. From the four postulates of quantum mechanics, there is an operator that corresponds to any physical quantity. In the case of absorption spectroscopy the corresponding operator is the Hamiltonian ($\hat{H}$), which includes the kinetic and potential energies of the molecule of interest. A molecule can undergo three types of transitions: electronic (hereafter denoted by subscript e) vibrational (subscript v), and rotational (subscript r), with $E_e > E_v > E_r$. The particular energy required to induce a transition can be given by the Schrödinger equation, which in general takes the form

$$\hat{H}(r, R)\Psi(r, R) = E_{evr}\Psi(r, R) \tag{1.1}$$

where Ψ represents the electronic wavefunction dependent on the electronic coordinate, r, and the nuclear coordinate, R, and E_{evr} is the total molecular energy. In addition, transitions are only allowed if they satisfy

$$\int \Psi_f \hat{\mu} \Psi_i d\tau \neq 0 \tag{1.2}$$

where Ψ_i is the initial state wavefunction of the transition, Ψ_f the final state wavefunction, and $\hat{\mu}$ is the electronic dipole moment operator. For infrared spectroscopy, this means to only transitions with an induced dipole moment (*e.g.*, an asymmetric stretch) can be observed.

The Schrödinger equation can only be solved exactly for the hydrogen atom. As such, for all other molecules a series of approximations are made in order to predict the molecular properties, such as the vibrational frequencies. In the simplest case the vibrational motion of molecules can be approximated as a harmonic oscillator; solving the Schrödinger equation for a harmonic oscillator gives the following energy levels:

$$E(v) = \sum_{i=1}^{3N-5} \left(v_i + \frac{1}{2}\right) \omega_e \tag{1.3}$$

where v_i is the vibrational level and ω_e is the equilibrium harmonic frequency. However, real molecular bonds are anharmonic oscillators, and the vibrational level spacings become closer as

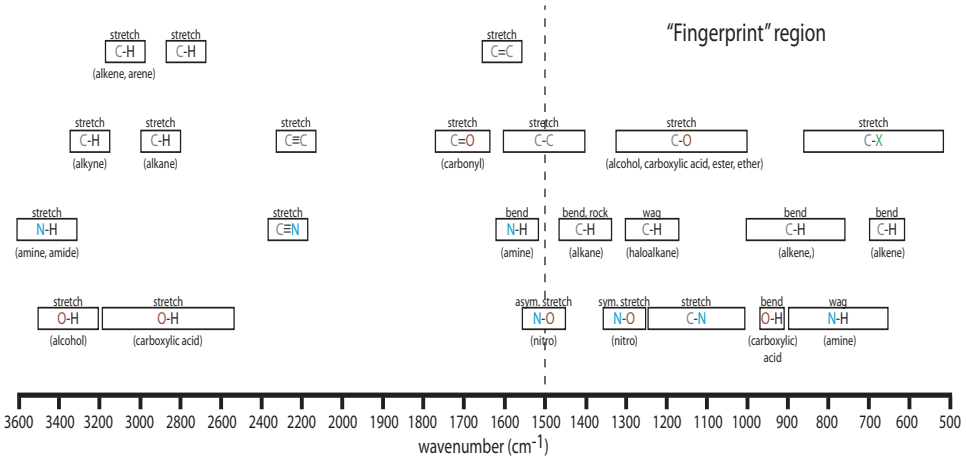

Figure 1.2: A chart of the characteristic frequency ranges for different vibrational motions, adapted from McMurry (2016).

v_i increases. To take this into account, the vibrational energy level equation can be described as a series expansion with successively higher order correction terms:

$$E(v) = \sum_{i=1}^{3N-5} \left(v_i + \frac{1}{2}\right) \omega_e + \sum_i \sum_{j \geqslant i} x_{ij} \left(v_i + \frac{1}{2}\right) \left(v_j + \frac{1}{2}\right) + \sum_i \sum_{j \geqslant i} g_{ij} l_i l_j + \text{h.o.t.} \tag{1.4}$$

where x_{ij} and g_{ij} are the anharmonicity constant between two states i and j, l is the vibrational angular momentum quantum number, and h.o.t. stands for higher order terms.

For a symmetric top molecule, which in the extreme case is a linear molecule, there are two types of vibrations: either the dipole moment remains along the intranuclear axis during the vibration, a parallel band, or the dipole moment becomes orthogonal to the intranuclear axis during the vibration, a perpendicular band. Furthermore, transitions of $\Delta v = 1$ from the ground state result in fundamental modes, while transitions of $\Delta v > 1$ result in overtone modes, and transitions involving more than one vibrational state results in a combination state.

Different vibrational motions have characteristic frequencies, based on the atoms and bonds involved (see Figure 1.2). For some vibrational motions, like stretching vibrations, all molecules in the same family have roughly the same vibrational frequency, which can make molecular identification ambiguous. However, some vibrational motions, like bending vibrations, are particular to the size and shape of the molecule making their frequencies more unique to a particular molecule (even between members of the same molecular family). These motions are typically at $\leqslant 1500$ cm^{-1}, which is aptly named the "Fingerprint" region.

In the gas-phase, transitions between vibrational levels include rotational transitions. The energy levels corresponding to rotational transitions can be approximated assuming the molecule is a rigid rotor. As such for symmetric top molecule (where linear molecules can be thought of as an extreme case, $K = 0$), the solution to the Schrödinger equation for pure rotation levels gives the following expression:

$$E(J, K, l) = BJ(J+1) + (A - B)K^2 + 2A\zeta l K \tag{1.5}$$

where J is the total angular momentum quantum number, K is the projection quantum number, ζ is the Coriolis coupling constant, and A and B are the rotational constants, such that for example

$$B = \frac{h}{8\pi^2 c I_B} = \frac{h}{8\pi^2 c \sum m_i r_i^2} \tag{1.6}$$

Real molecules are not perfectly rigid, and when they rotate, centrifugal stretching changes the spacing between the rotational levels. Taking into account the correction terms, the rotational energy level equation becomes:

$$E(J, K, l) = BJ(J+1) + (A-B)K^2 + 2A\zeta lK - D_J J^2(J+1)^2 - D_{JK}J(J+1)K^2 - D_K K^4 \quad (1.7)$$

where D_J, D_{JK}, and D_K are the centrifugal distortion constants, and for a linear molecule $K = 0$. Allowed pure rotational transitions are between $\Delta J = \pm 1$ and $\Delta K = 0$.

Combining the vibrational and rotational parts gives the energy level equation for ro-vibrational transitions:

$$E(v, J, K, l) = \sum_{i=1}^{3N-5}\left(v_i + \tfrac{1}{2}\right)\omega_e + \sum_i \sum_{j \geqslant i}\left(v_i + \tfrac{1}{2}\right)\left(v_j + \tfrac{1}{2}\right)x_{ij} + BJ(J+1) \quad (1.8)$$

$$+(A-B)K^2 + 2A\zeta lK - D_J J^2(J+1)^2 - D_{JK}J(J+1)K^2 - D_K K^4$$

For a particular vibrational state the vibrational dependent rotational constants are given by:

$$A_v = A_e - \sum_i \alpha_i^A\left(v_i + \tfrac{d_i}{2}\right) \sim A_o - \sum_i (v_i \alpha_i^A) \quad (1.9a)$$

$$B_v = B_e - \sum_i \alpha_i^B\left(v_i + \tfrac{d_i}{2}\right) \sim B_o - \sum_i (v_i \alpha_i^B) \quad (1.9b)$$

where α is the vibration-rotation interaction constant that can be used to identify the molecule and vibrational states involved in an observed ro-vibrational band.

For a parallel band of a symmetric top molecule, selection rules allow ro-vibrational transitions are between states where

$\Delta K = 0$ and $\Delta J = 0, \pm 1$ if $K \neq 0$
$\Delta K = 0$ and $\Delta J = \pm 1$ if $K = 0$

Conversely, for a perpendicular band of a symmetric top molecule allowed transitions are only allowed for

$$\Delta K = \pm 1 \text{ and } \Delta J = 0, \pm 1$$

The selection rules for linear molecules have no K dependencies, however, they do depend on l. Transitions are allowed for $\Delta l = 0, \pm 1$. If both the upper and lower states are $l = 0$ (Σ states) then the selection rules only allow transitions for

$$\Delta J = \pm 1$$

However, if in either the upper or lower state $l \neq 0$ then transitions are allowed for

$$\Delta J = 0, \pm 1$$

If the molecule has a center of inversion, then transitions are only allowed between states with opposite symmetries (*i.e.*, g [symmetric] $\leftrightarrow$ u [asymmetric]).

The general structure of infrared ro-vibrational bands includes a series of transitions that can be broken up into the P-branch (ΔJ = -1), the Q-branch (ΔJ = 0), and the R-branch (ΔJ = +1); see Figure 1.3. The rotational transition intensities are determined by the Hönl-London factors and the level populations (N_J), which are governed by Boltzmann distribution

$$N_J = g(2J+1)\exp(-E/k_B T) \quad (1.10)$$

where k_B is the Boltzmann constant, T is the rotational temperature of the molecule, and g is the degeneracy.

The degeneracy is an effect of the nuclear spin on the rotational level population. For molecules

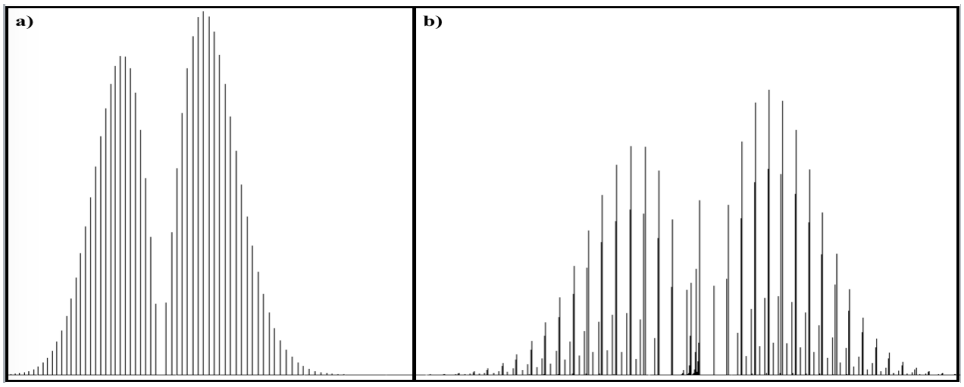

Figure 1.3: An example of a simulated a) linear parallel (Σ - Σ) band with P- and R-branches, and b) symmetric top molecule parallel (A_1 - A_1) band with P-,Q-, and R-branches. Both simulated spectra have the same rotational temperature of 20 K.

with a center of inversion (*e.g.*, acetylene, HC_2H or C_3) the degeneracies for the totally symmetric and totally antisymmetric levels differ, and result in observed intensity alternation of the ro-vibrational transitions. The degeneracies are given by:

$$g_{\text{symmetric}} = (2I+1)(I+1) \tag{1.11a}$$

$$g_{\text{antisymmetric}} = (2I+1)I \tag{1.11b}$$

where I is the spin angular momentum quantum number, which is a whole integer for Bosons (*e.g.*, for C, I = 1) and is a half integer for Fermions (*e.g.*, for H, I = 1/2). Conversely, for molecules without a center of inversion (*e.g.*, propyne, $CH_3C{\equiv}CH$) the degeneracies for both symmetric and asymmetric levels are given by:

$$g = (2I_A+1)(2I_B+1) \tag{1.12}$$

The intensity of the transitions can also be effected by anharmonic perturbations (*e.g.*, Fermi resonances and Coriolis coupling). A perturbation is the result of the wavefunctions of two modes with similar energy mixing in such a way that the two resulting modes can be described by a linear combination of the two original modes. The two resulting modes are shifted relative to the original modes such that they are pushed apart. In addition, the wavefunction mixing can result in intensity changes, such as intensity borrowing that allows a previously "dark" or forbidden state having observable transitions.

1.3 *ab initio* METHODS TO PREDICT SPECTROSCOPIC PARAMETERS

To predict where the ro-vibrational transitions of astrophysically relevant molecules are expected *ab initio* calculations were performed with the development version of the CFOUR (Coupled-Cluster techniques for Computational Chemistry) program (CFOUR, 2017). The calculations in this thesis were performed using the coupled cluster singles and doubles excitation with a perturbative treatment of triples excitation (CCSD(T)) method. In CC theory the wavefunction, $|\Psi_{CC}\rangle$, is given by the exponential ansatz

$$|\Psi_{CC}\rangle = e^{\hat{T}}\,|\Phi_0\rangle \tag{1.13}$$

where $|\Phi_0\rangle$ is the reference wavefunction, a Slater determinant usually constructed from Hartree-Fock molecular orbitals, and $\hat{T}$ is the cluster operator. It is a post Hartree-Fock method that accounts for electron correlation to approximate the exact energy given in the Schrödinger equation.

With a sufficiently large basis set, CCSD(T) has been shown to accurately reproduce experimental spectroscopic parameters of semi-rigid molecules (Raghavachari et al., 1989; Gauss & Stanton, 1997), and is, in general, called the "gold standard" of computation chemistry.

The correlation consistent polarized X-ζ basis set (cc-pVXZ; where X = D, T, Q, 5, etc) developed by Dunning and co-workers are built upon a core of Hartree-Fock orbitals, and are designed to converge systematically and smoothly to the complete basis set limit with successively more basis functions. Moreover, the core correlation set (cc-pCVXZ) uses all electrons (AE) and all orbitals (occupied as well as virtual), which is needed for accurate geometry determination. The equilibrium geometries of the molecules studied were determined using the large cc-pCVQZ (quadruple zeta), which features the truncations of [8s7p5d3f1g] (non-hydrogen atoms) and [4s3p2d1f] (hydrogen) of the (15s9p5d3f1g) and (6s3p2d1f) primitive basis set, respectively (Woon & Dunning Jr., 1995; Feller, 1996; Schuchardt et al., 2007). (AE)-CCSD(T)/cc-pCVQZ has been shown to give very accurate equilibrium geometries for unsaturated hydrocarbons (Auer & Gauss, 2001; Bak et al., 2001; Zhang et al., 2007; Simmonett et al., 2009).

The equilibrium geometry calculations, including determination of the equilibrium rotational constants, were done by searching for a minimum on the potential energy surface (PES) using analytic energy derivatives within a Quasi-Newton scheme (Stanton & Gauss, 2000). The calculations start with a unit matrix in the first iteration that is updated using the BFGS scheme. The molecular equilibrium geometry is considered converged when the root-mean-square (rms) gradient fell below 10^{-10} au.

However, it is well known that correlation-consistent basis sets, such as cc-pCVQZ, tend to underestimate the vibrational frequencies of symmetric bending modes (π_g) of conjugated molecules due to their susceptibility to an intramolecular variant of basis set superposition error (BSSE), *i.e.*, when different parts of the same molecule approach one another their basis functions overlap (Simandiras et al., 1988). It has been shown that one way to avoid this problem is to use basis sets with a large number of Gaussian primitives (particularly f-type), such as the atomic natural orbital (ANO) basis set (which has the primitive basis set (13s8p6d4f2g) for non-hydrogen atoms and (8s6p4d2f) for hydrogen) (Almlöf & Taylor, 1987; Bauschlicher Jr. & Taylor, 1993; Martin et al., 1998). The basis set has a common truncation: [4s3p2d1f] for non-hydrogen atoms and [4s2p1d] for hydrogen (hereafter known as ANO1, which is used in this thesis) (Almlöf & Taylor, 1987; Feller, 1996; Schuchardt et al., 2007). Furthermore, the basis set is used such that only the occupied valence orbitals and all virtual orbitals of carbon are considered, *i.e.*, standard frozen-core (fc) calculation. This is because (fc)-CCSD(T)/ANO1 has been shown to accurately reproduce experimental IR frequencies and intensities for small molecules (Martin et al., 1997, 1998; Vázquez & Stanton, 2007).

At the (fc)-CCSD(T)/ANO1 optimized geometry, calculations of the harmonic vibrational frequencies and IR intensities were determined using finite difference of analytic gradients in parallel, starting from the harmonic oscillator, rigid-rotor approximation. Subsequently, the anharmonic vibrational frequencies, IR intensities, vibration-rotation interaction constants (α), and Fermi resonances were determined from full cubic and the semidiagonal part of the quartic force fields obtained by numerical differentiation of analytic CCSD(T) second derivatives using second-order vibrational perturbation (VPT2) theory that also starts from the harmonic oscillator, rigid-rotor approximation (Gauss & Stanton, 1997; Matthews et al., 2007). For most of the calculations carried out in this thesis, the following thresholds for convergence were used: 1) the SCF equations are considered converged when the maximum change in density matrix elements is less than 10^{-10}, 2) the CC amplitudes are considered converged when the maximum of all changes in the amplitudes is less than 10^{10}, and 3) the linear equations' smallest residual falls below 10^{-10}.

CCSD(T) can be computationally expensive for large molecules, and thus for the theoretical study of PAHs the relatively less accurate, but computationally inexpensive density functional theory (DFT) method was used. DFT uses a functional (the electron density) instead of the wavefunctions to approximate the solution of the Schrödinger equation.

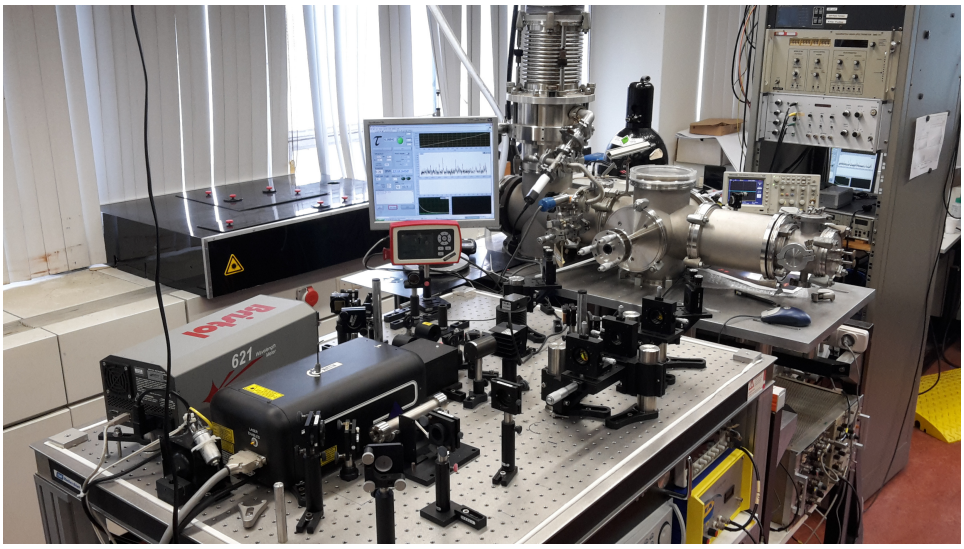

Figure 1.4: The SPIRAS setup at the Sackler Laboratory for Astrophysics at Leiden Observatory.

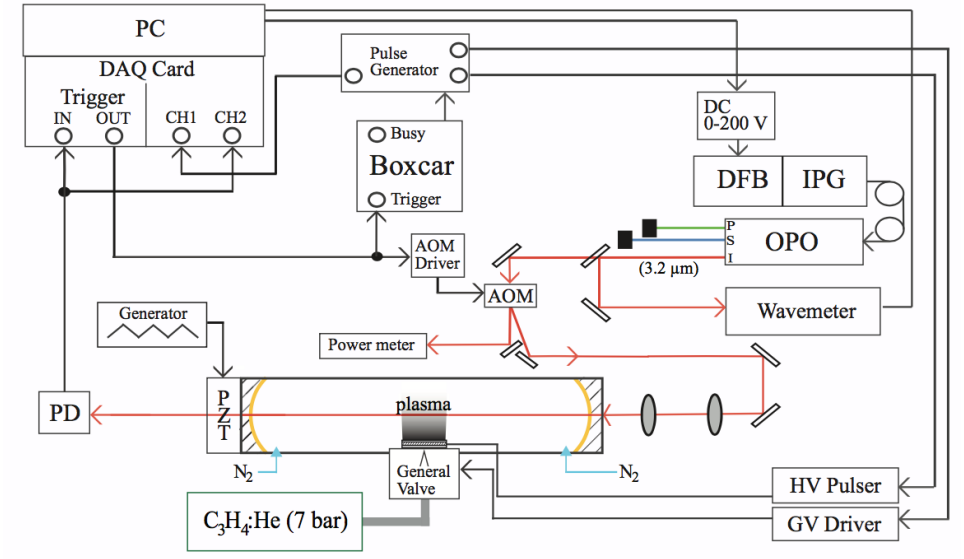

Figure 1.5: Adapted from Zhao et al. (2013), the box diagram of the SPIRAS set up. DFB: distributed feedback fiber laser; IPG: fiber amplifier; OPO: optical parametric oscillator; I: idler beam; S: signal beam; P: pump beam; AOM: acousto-optic modulator; GV: general valve driver; HV: high voltage pulser; PZT: piezoelectric transducer; PD: photovoltaic detector.

1.4 EXPERIMENTAL MEASUREMENTS OF RO-VIBRATIONAL SPECTRA

To measure the experimental spectra of astrophysically relevant molecules, the supersonic plasma infrared absorption spectrometer (SPIRAS) at the Sackler Laboratory for Astrophysics was used (Figure 1.5); the experimental setup details are taken from Zhao et al. (2013) and exact experimental settings are given in the relevant chapters.

The main chamber of SPIRAS is formed using a six-way standard ISO160 vacuum chamber mounting the optical cavity and discharge nozzle, and is kept at a stagnation pressure of ~0.007 mbar by a vacuum system with a pumping capacity of 4800 m^3/hour. The analytes, or molecules of study, are introduced into the main chamber through a slit discharge nozzle that is mounted in the center of the main chamber with the slit exit parallel to, and upstream from the axis of the optical cavity. The nozzle is based on the design of Motylewski & Linnartz (1999) (shown in detail in Figure 1.6), and consists of multiple layers starting with a 2 mm pinhole pulsed valve (General Valve, Series 9), followed by a multi-channel body consisting of a series of pin-holes of varying size that regulates the gas distribution towards the exit. The nozzle can be switched to produce either a pulsed and continuous gas flow.

The slit exit is formed by a layered ceramic insulator-anode-ceramic insulator-cathode system.

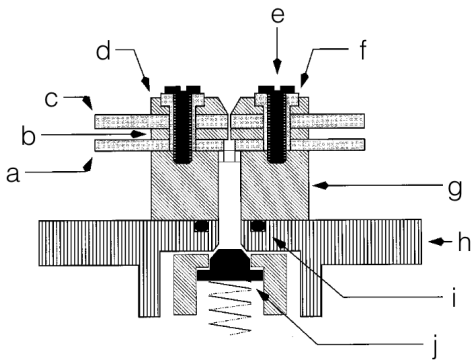

Figure 1.6: Adapted from Motylewski & Linnartz (1999), the schematic of the SPIRAS slit discharge nozzle. a) ceramic insulator plate with 0.5 × 20 mm slit opening, b) anode plate with 0.5 × 20 mm slit opening, c) ceramic insulator place with 0.3 × 30 mm slit opening, d) one of the metal jaws that make up the cathode, e) screw, f) ceramic screw insulator, g) multi-channel body that consists of a hollow body and six pin-hole openings at the top that have varying diameters that get progressively smaller from outside to inside, h) 2 mm pinhole General Valve, i) O-ring, j) Teflon poppit.

The cathode is composed of two metal plates, or "jaws", which have a 45 degree edge positioned ~0.1 mm away from the edge of the insulator slit edge. The thin slit results in the gas flow being planar instead of conical, and reduces the Doppler broadening of the absorption lines. Furthermore, the precursor gas typically has a backing pressure of a few bars before the nozzle. The large difference between the main chamber stagnation pressure and the backing pressure results in a supersonic expansion of the gas, which results in effective adiabatic cooling and lower Doppler broadening of the molecules in the jet. When necessary, a negative high voltage, typically -400 - -700 V, is applied to the cathode resulting in a plasma discharge.

SPIRAS uses continuous wave cavity ring-down spectroscopy (cw-CRDS) to measure the IR spectrum of the analytes, which are for this work astrophysically relevant hydrocarbon molecules. Cw-CRDS uses a pulse of light from a continuous wave laser as the light source for absorption spectroscopy. This spectroscopic method allows for the high detection sensitivity (absorption, A, ~10^{-6} cm^{-1}) needed to study the hydrocarbon molecules of astrophysical interest, particularly

Figure 1.7: A typical acetylene plasma expansion produced from the SPIRAS slit discharge nozzle.

compared to direct or multi-pass absorption spectroscopy. This is achieved by using two highly reflective mirrors (~99.97% at 3 μm, 1 m radius plano-concave) spaced 56 cm apart to form the optical cavity, effectively trapping light inside the cavity, and increasing the absorption path length through the analyte. The signal-to-noise (S/N) is further enhanced by measuring the light that leaks out of the cavity as a function of time, which means the measurements are insensitive to intensity fluctuations in the light source. The 1/e decay time of the light (called the ring-down lifetime) for CRDS can be expressed as:

$$\tau = \frac{L}{c}\frac{1}{(1-R)+\alpha l} \tag{1.14}$$

where c is the speed of light, L is the cavity length, α is the absorptivity constant, l is the path length, and R is the reflectivity of the mirrors. In an empty cavity the ring-down time (τ_0) is a measure of the loss of light due to the mirrors, and for most low pressure gases extinction due to scattering is negligible, so the absorbance can be written as

$$A = \alpha l = \frac{L}{c}\left(\frac{1}{\tau} - \frac{1}{\tau_0}\right) \tag{1.15}$$

As such, the greater the value of τ the more sensitive the detection. For SPIRAS, operating around 3 μm, typically τ_0 is 9 μs, but given the wavelength dependent reflectivity of the mirrors it can be up to 18 μs.

The narrowband mid-IR light source used on SPIRAS is produced by a combination pump laser and continuous wave optical parametric oscillator (cw-OPO) system. The output of a DFB fiber laser (NKT photonics, Koheras Basik Y-10) is amplified in a fiber amplifier (IPG Phtonics, YAR-10K-1064-LP-SF) to give an output power of 10 W. The light is then carried as the pump source through an optic fiber to the single-mode cw-OPO (Aculight Argos 2400SF; module B for λ = 2.5 - 3.2 μm or module C for λ = 3.2 - 3.9 μm). The cw-OPO unit converts the pump laser into two additional lower energy laser beams, the signal and the idler beams, by a periodically-poled lithium niobate (PPLN) crystal, such that

$$\frac{1}{\lambda_{pump}} = \frac{1}{\lambda_{signal}} + \frac{1}{\lambda_{idler}} \tag{1.16}$$

The output signal and residual pump beam are sent to beam dumps and discarded, while the idler beam is directed towards the optical cavity and used for the experiment. The continuous tunability of the wavelength is accomplished through a number of methods. Course tuning of the wavelength is done using the etalon and crystal inside the optical cavity of the OPO. Rotation of the etalon changes the angle of incidence of the signal laser, and allows for the frequency to be changed in steps of approximately 1 cm^{-1}. Varying where the laser crosses the crystal inside the OPO can change the phase-matching conditions, and translating the crystal linearly results in frequency jumps of about 10 cm^{-1}. The finest level of tuning is done using a LabVIEW program to change the voltage applied to the piezo-electric transducer (PZT) attached to the seed laser. For

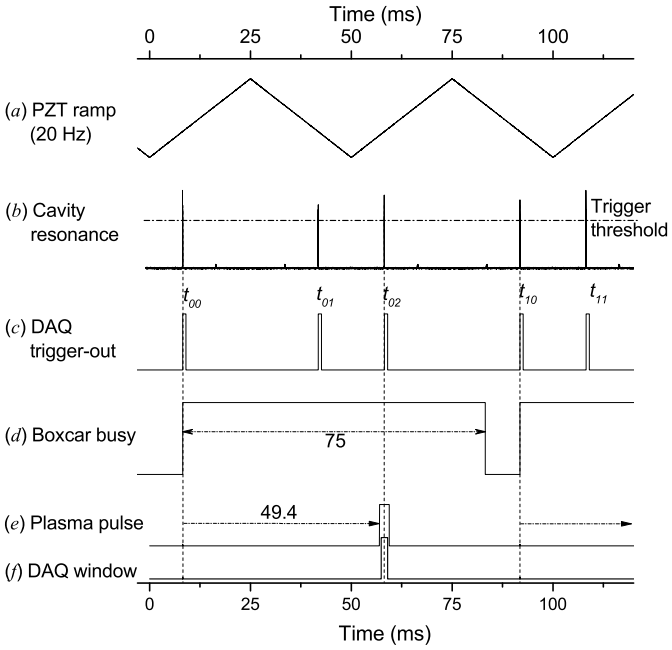

Figure 1.8: The triggering scheme used in the experiment, adapted from (Zhao et al., 2013). a) The triangular function of the applied voltage to the PZT altering the cavity length. b) Traces the cavity modes, where a spike is when the cavity is in resonance. c) Traces the TTL signals generated by the DAQ when the light intensity surpasses the preset threshold level. d) The Boxcar busy window which is generated by the TTL signal sent from DAQ trigger out at t_{00}. e) Traces the plasma pulse and f) traces the DAQ acquisition window generated by they rising edge of the Boxcar busy signal. Only the cavity resonance at t_{02} will initiate a measured ring-down event.

one scan the applied voltage is increased from about 90 to 195 V, which changes the idler frequency by up to 1.4 cm^{-1}.

The idler beam, in the 3 μm range, has a total output power of about 1.2 W, an effective bandwidth of less than 1 MHz, and a mode structure that is purely TEM_{00}. The idler is sent through a beam splitter after it exits the cw-OPO cavity, and roughly 1% of the beam is directed to a continuously self-calibrated wavemeter (Bristol 621-A), to measure the frequency. The remainder of the idler is directed through an acousto-optic modulator (AOM), which when on generates an acoustic wave that diffracts the laser beam into the fundamental and higher orders. The first-order deflection is spatially separated from the fundamental by an angle of ~15 degrees, and it is this 10% of the idler that is coupled into the main chamber.

Perfect mode matching the laser to the optical cavity will give the peak light intensity, and limits interference by modes other than the TEM_{00}. To mode match the laser's wavelength the cavity length is varied by a PZT mounted on the back of the far mirror, and the cavity length is modulated by an applied triangular function voltage. The period and amplitude of the applied voltage is chosen such that the cavity is transparent to infrared light twice during one period (once on the raising edge and once on the falling edge, Figure 1.8).

The light intensity out of the cavity is detected by an IR-photovoltaic detector (Vigo System S.A., PVI-3TE-5, 50 MHz), and a signal is then sent from the detector to both the signal and trigger input channels of a fast data acquisition (DAQ) card equipped in a computer. In the most general case, when the intensity of the light in the cavity reaches a threshold value, a trigger is sent to the

DAQ card, which generates a transistor-transistor logic (TTL) pulse. The TTL signal is then sent to the AOM driver, switching off the AOM leaving only the fundamental. This gives a "pulse" of light, triggering a ring-down event.

In the past, software-based trigger schemes were used to coincide gas/plasma pulses with ring-down events, but they were relatively complex and inefficient (Birza et al., 2002). SPIRAS instead uses a hardware-based timing and multi-trigger scheme that results in more than 90% of the plasma pulses measured; trigger scheme details are shown in Figure 1.8.

For a given modulation frequency, *e.g.*, 15 kHz, the first time the cavity is in resonance the DAQ card generates a TTL pulse, marked as t_{00}, which is sent to both the AOM driver and a Boxcar gated integrator (SRS, SR250). The AOM driver switches off the AOM, while the Boxcar gated integrator simultaneously generates a 75 ms wide TTL pulse at its busy output channel (henceforth called the busy gate) and the rising edge of the busy gate is used to trigger a multichannel pulse generator. The width of the busy gate is chosen to be for a duration greater than the period of the PZT ramp, such that it covers at least two cavity resonances: the resonance on the falling PZT ramp, t_{01}, and a second rising resonance, t_{02}. The multichannel pulse generator has a built-in delay that is used to trigger the gas valve driver and high voltage pulser at about one period after t_{00}. The pulse generator also sends a TTL signal synchronized with the HV pulse, but with a narrower width, to the second input channel of the DAQ card. This is the data acquisition time window, if a resonance falls within this window a ring-down event is measured.

The use of a Boxcar integrator avoids the need for an extensive programming code for a software interface with the pulsed plasma generation, and this simplifies data acquisition. Approximately 10 - 14 plasma pulses are effectively generated and measured per second. Non-detections mainly occur in the case that cavity resonances are too close to the turning points of the PZT-sweep, trace a in Figure 1.8. A typical ring-down time ranged from about 5 - 15 µs depending on the laser frequency. To further reduce the noise, such as that due to inconsistent gas pulse pressures, fifteen ring-down times are averaged per wavenumber. The final absorption spectrum is recorded by plotting the ring-down time as a function of laser frequency.

1.5 THIS THESIS

This thesis is about the study of astrophysically relevant hydrocarbons through infrared spectroscopy. All of the molecules studied are believed to be or have been detected in astronomical environments. The experiments and theoretical calculations detailed here were primarily carried out at the Sackler Laboratory for Astrophysics at Leiden University, with some theoretical work done out at the University of Texas at Austin and some experimental work performed at the University of Science and Technology of China, and the astronomical infrared spectra were taken using the AKARI space telescope. This thesis is organized as follows: The theory of hydrocarbon infrared spectroscopy is given through the computational study of small polyynes [$HC_{2n}H$] and propyne [CH_3CCH]. The theory is then tested through experimental studies of diacetylene [HC_4H], triacetylene [HC_6H], propyne [CH_3CCH], and cyclopropenyl cation [c-$C_3H_3^+$]. Finally, experimental spectra and theory are applied to identify deuterated PAHs [D_n-PAHs] in the interstellar medium (ISM). Through comparison of astronomical spectra and this laboratory or theoretical work adds insight into the physical chemistry of astronomical environments.

Chapters 2, 3 and 4

Long chain unsaturated hydrocarbons are fairly abundant in carbon-rich environments, *e.g.*, the atmosphere of Titan or the protoplanetary nebulae CRL 618 and SMP LMC 11. In fact, chains have been observed of C_nH (Bell et al., 1999) and HC_nCN (Bell et al., 1992) up to n = 8. Interestingly though, polyynes [HC_nH] have only been observed for chain lengths up to n = 6. We present high resolution experimental spectra of diacetylene [HC_4H], and triacetylene [HC_6H] in the 3 µm region, which includes the C-H asymmetric stretch fundamental and a number of sequence bands. In

addition, we present CCSD(T) calculations for acetylene [HC_2H] and the three smallest polyynes: diacetylene [HC_4H], triacetylene [HC_6H], and tetraacetylene [HC_8H]. The predicted vibrational frequencies and rotational constants agree well with high resolution experimental data for HC_2H, HC_4H, and HC_6H, and suggests similar accuracies for HC_8H. Based on the calculated parameters, the lack of detection of HC_8H in astronomical sources is likely a result of spectral overlap of transitions of HC_8H with transitions of the more abundant HC_4H and HC_6H. This work appears in Zhao et al. (2014), Doney et al. (2015) and Doney et al. (2018b).

Chapter 5 and 6

Another abundant acetylenic hydrocarbon is propyne [H_3CCCH], which has been seen in for example the atmosphere of Titan, in SMP LMC 11, and in the warm dense gas around the low-mass protostar IRAS 16293-2422. Due to the close spacings of the *K*'-subband transitions, propyne is a good probe of the interstellar kinetic temperature. We present high resolution spectra of the ν_1 acetylenic C-H stretch fundamental and the $\nu_3+\nu_5$ combination band of normal isotopologue of propyne, and the ν_1 acetylenic C-H stretch fundamental of the three mono-substituted ^{13}C isotopologues. For the ^{13}C isotopologues this is the first rotationally resolved measurement of the ν_1 fundamentals, and a full rotational analysis is given to highlight the effect of isotopic position in the carbon chain on anharmonic perturbations. CCSD(T) calculations for all four isotopologues are presented to support the identification and analysis of the new ro-vibrational bands. This work appears in Doney et al. (2017) and Doney et al. (2018a).

Chapter 7

In most astronomical hydrocarbon chemical networks carbocations are the key intermediates. However, a lack of accurate line positions make their astronomical identification difficult. We present the first high resolution measurement of the cyclopropenyl cation [c-$C_3H_3^+$]; through its ν_4 C-H stretch fundamental band. The resulting ground state spectroscopic parameters are sufficiently accurate to help astronomical searches for this molecule in both the infrared and submillimeter. This work appears in Zhao et al. (2014).

Chapter 8

In the interstellar medium, the gas-phase D/H ratio is too low to be explained by stellar processing alone. As such, it is believed that some of the missing deuterium is locked up in either dust grains or in molecules. PAHs are good reservoirs for deuterium, due to their relatively stability against photodissociation (meaning they are long-lived, and thus ubiquitous molecule in the interstellar medium) and their large size ($N_C > 50$; meaning that a large number of deuterium can be incorporated into the molecule) Peeters et al. (2004) made the first tentative detection of deuterated PAHs in the Orion Bar and M17 using The Infrared Space Observatory (ISO). Using the AKARI satellite we have confidently observed deuterated PAHs in an addition six Milky Way sources. The comparison between DFT calculations and observations show that the deuterium preferentially add aliphatically to the PAH frame, and that the addition is extremely environmentally dependent. This work appears in Doney et al. (2016).

1.6 BIBLIOGRAPHY

Agúndez, M., Cernicharo, J., Quintana-Lacaci, G., et al. 2017, Astronomy & Astrophysics, 601, A4
Allamandola, L. J., Tielens, A. G. G. M., & Barker, J. R. 1989, The Astrophysical Journal Supplements, 71, 733
Almlöf, J. & Taylor, P. R. 1987, The Journal of Chemical Physics, 86, 4070
Araki, M., Takano, S., Sakai, N., et al. 2017, The Astrophysical Journal, 847, 51
Auer, A. A. & Gauss, J. 2001, Physical Chemistry Chemical Physics, 3, 3001
Bak, K. L., Gauss, J., Jørgensen, P., et al. 2001, The Journal of Chemical Physics, 114, 6548
Bauschlicher Jr., C. W. & Taylor, P. R. 1993, Theoretica Chimica Acta, 86, 13
Bell, M. B., Avery, L. W., MacLeod, J. M., & Matthews, H. E. 1992, The Astrophysical Journal, 400, 551
Bell, M. B., Feldman, P. A., Watson, J. K. G., et al. 1999, The Astrophysical Journal, 518, 740

Birza, P., Motylewski, T., Khoroshev, D., et al. 2002, Chemical Physics, 283, 119
Cernicharo, J., Daniel, F., Castro-Carrizo, A., et al. 2013, The Astrophysical Journal Letters, 778, L25
Cernicharo, J. & Guélin, M. 1996, Astronomy & Astrophysics, 309, L27
Cernicharo, J., Heras, A. M., Tielens, A. G. G. M., et al. 2001, The Astrophysical Journal Letters, 546, L123
CFOUR. 2017, Coupled-Cluster techniques for Computational Chemistry, a quantum-chemical program package by J.F. Stanton, J. Gauss, M.E. Harding, P.G. Szalay with contributions from A.A. Auer, R.J. Bartlett, U. Benedikt, C. Berger, D.E. Bernholdt, Y.J. Bomble, L. Cheng, O. Christiansen, F. Engel, R. Faber, M. Heckert, O. Heun, C. Huber, T.-C. Jagau, D. Jonsson, J. Jusélius, K. Klein, W.J. Lauderdale, F. Lipparini, D.A. Matthews, T. Metzroth, L.A. Mück, D.P. O'Neill, D.R. Price, E. Prochnow, C. Puzzarini, K. Ruud, F. Schiffmann, W. Schwalbach, C. Simmons, S. Stopkowicz, A. Tajti, J. Vázquez, F. Wang, J.D. Watts and the integral packages MOLECULE (J. Almlöf and P.R. Taylor), PROPS (P.R. Taylor), ABACUS (T. Helgaker, H.J. Aa. Jensen, P. Jørgensen, and J. Olsen), and ECP routines by A. V. Mitin and C. van Wüllen. For the current version, see http://www.cfour.de.
Cherchneff, I. 2011, in EAS Publications Series, Vol. 46, EAS Publications Series, ed. C. Joblin & A. G. G. M. Tielens, 177–189
Chuang, K.-J., Fedoseev, G., Ioppolo, S., van Dishoeck, E. F., & Linnartz, H. 2016, Monthly Notices of the Royal Astronomical Society, 455, 1702
Churchwell, E. & Hollis, J. M. 1983, The Astrophysical Journal, 272, 591
Doney, K. D., Candian, A., Mori, T., Onaka, T., & Tielens, A. G. G. M. 2016, Astronomy & Astrophysics, 586, A65
Doney, K. D., Zhao, D., Bouwman, J., & Linnartz, H. 2017, Chemical Physics Letters, 684, 351
Doney, K. D., Zhao, D., & Linnartz, H. 2015, Journal of Molecular Spectroscopy, 316, 54
Doney, K. D., Zhao, D., & Linnartz, H. 2018a, The Journal of Physical Chemistry A, 122, 582
Doney, K. D., Zhao, D., Stanton, J. F., & Linnartz, H. 2018b, Physical Chemistry Chemical Physics
Feller, D. 1996, Journal of Computational Chemistry, 17, 1571
Gauss, J. & Stanton, J. F. 1997, Chemical Physics Letters, 276, 70
Gibb, E. L., Van Brunt, K. A., Brittain, S. D., & Rettig, T. W. 2007, The Astrophysical Journal, 660, 1572
Kim, S. J., Caldwell, J., Rivolo, A. R., Wagener, R., & Orton, G. S. 1985, Icarus, 64, 233
Malek, S. E., Cami, J., & Bernard-Salas, J. 2012, The Astrophysical Journal, 744, 16
Martin, J. M. L., Lee, T. J., & Taylor, P. R. 1998, The Journal of Chemical Physics, 108, 676
Martin, J. M. L., Taylor, P. R., & Lee, T. J. 1997, Chemical Physics Letters, 275, 414
Matthews, D. A., Vázquez, J., & Stanton, J. F. 2007, Molecular Physics, 105, 2659
McEwan, M. J., Scott, G. B. I., Adams, N. G., et al. 1999, The Astrophysical Journal, 513, 287
McMurry, J. 2016, Organic Chemistry, 9th edn. (Cengage Learning)
Motylewski, T. & Linnartz, H. 1999, Review of Scientific Instruments, 70, 1305
Müller, H. S., Schlöder, F., Stutzki, J., & Winnewisser, G. 2005, Journal of Molecular Structure, 742, 215
O'Keefe, A. & Deacon, D. A. G. 1988, Review of Scientific Instruments, 59, 2544
Papadopoulos, P. P. 2007, The Astrophysical Journal, 656, 792
Peeters, E., Allamandola, L. J., Bauschlicher Jr., C. W., et al. 2004, The Astrophysical Journal, 604, 252
Raghavachari, K., Trucks, G. W., Pople, J. A., & Head-Gordon, M. 1989, Chemical Physics Letters, 157, 479
Sakai, N. & Yamamoto, S. 2013, Chemical Reviews, 113, 8981
Schuchardt, K. L., Didier, B. T., Elsethagen, T., et al. 2007, Journal of Chemical Information and Modeling, 47, 1045
Simandiras, E. D., Rice, J. E., Lee, T. J., Amos, R. D., & Handy, N. C. 1988, The Journal of Chemical Physics, 88, 3187
Simmonett, A. C., Schaefer III, H. F., & Allen, W. D. 2009, The Journal of Chemical Physics, 130, 044301
Smith, D. 1992, Chemical Reviews, 92, 1473
Stanton, J. F. & Gauss, J. 2000, International Reviews in Physical Chemistry, 19, 61
van Kempen, T. A., van Dishoeck, E. F., Salter, D. M., et al. 2009, Astronomy & Astrophysics, 498, 167
Vázquez, J. & Stanton, J. F. 2007, Molecular Physics, 105, 101
Waite, J. H., Young, D. T., Cravens, T. E., et al. 2007, Science, 316, 870
Wakelam, V., Herbst, E., Loison, J.-C., et al. 2012, The Astrophysical Journal Supplement Series, 199, 21
Winnewisser, G. & Walmsley, C. M. 1978, Astronomy & Astrophysics, 70, L37
Woon, D. E. & Dunning Jr., T. H. 1995, The Journal of Chemical Physics, 103, 4572
Zhang, X., Maccarone, A. T., Nimlos, M. R., et al. 2007, The Journal of Chemical Physics, 126, 044312
Zhao, D., Doney, K. D., & Linnartz, H. 2014, Journal of Molecular Spectroscopy, 296, 1
Zhao, D., Doney, K. D., & Linnartz, H. 2014, The Astrophysical Journal Letters, 791, L28
Zhao, D., Guss, J., Walsh, A. J., & Linnartz, H. 2013, Chemical Physics Letters, 565, 132